



Contents lists available at ScienceDirect

Journal of Volcanology and Geothermal Research

journal homepage: www.elsevier.com/locate/jvolgeores

Evolution of crystal sizes in the series of dissolution and precipitation events in open magma systems

A.G. Simakin ^{a,*}, I.N. Bindeman ^b^a Institute of Experimental Mineralogy RAS, Chernogolovka, Moscow Oblast, 142432, Russia^b Geological Sciences, 1272 University of Oregon, OR 97403-1272, USA

ARTICLE INFO

Article history:

Received 14 January 2008

Accepted 21 July 2008

Available online 30 July 2008

Keywords:

zircon

quartz

crystallization

ripening

Bishop tuff

Yellowstone

caldera-forming eruption

ABSTRACT

We propose a model that describes the evolution of crystal sizes and crystal size distributions (CSD) of igneous phenocrysts in a sequence of dissolution and crystallization events. This model is based on the assumption that crystal dissolution is rate-limited by diffusion in melt while crystal growth is controlled by the slower kinetic of new nucleation and growth. As a result, the dissolution rate is inversely proportional to crystal size coming into effect through the curvature of the crystal's surface, but the growth rate does not depend on the crystal size. Closed-form analytical solution of equation for CSD is obtained. We apply results of modeling to quartz and zircon, two prime minerals in silicic igneous systems that are widely used in geochemical and isotopic investigations. The time-series of multiple solution–reprecipitation episodes generate concave-downward CSDs and this result fits well with experimental and natural observations on the abundant concave-down CSD in silicic igneous rocks. We suggest that maturation of crystal populations with sizes above several micrometers can not be caused by a size effect on the solubility of the crystals (Ostwald ripening), but is rather driven by thermal oscillations in experiments and in nature. The model predicts that mean crystal size increases with time proportionally to $\sim t^{0.20}$, which is very close to the published experimental results for quartz maturation with the exponent of 0.19–0.22. Our proposed model gives an opportunity to use natural CSDs for interpretation of pre-eruptive magma history, when solubilities and diffusion data are available for constituent elements of the dissolving mineral. In particular, we present time estimates for maturing zircon populations in large volume ignimbrites and estimate that it takes 100–1000 yrs to mature an initially exponential CSD to a lognormal CSD.

© 2008 Elsevier B.V. All rights reserved.

1. Introduction

Magmatic crystals are extensively used for trace elemental and isotopic studies in many applications of petrology and geochemistry. With the advance, and with easy accessibility of in situ microbeam techniques such as electron- and ion microprobes, and laser ablation ICP-MS, the picture of chemical and isotope zoning and disequilibria has arisen (e.g., Davidson et al., 2007; Putirka and Tepley, in press). Cathodoluminescent imaging of quartz and zircon for example, records single or multiple solution–reprecipitation episodes that record temperature fluctuations as demonstrated recently using utilized Ti concentrations in these two minerals (e.g., Anderson et al., 2000; Hoskin and Schaltegger 2003; Watson and Harrison 2005; Wark and Watson, 2006).

Surprisingly, textural characterizations of igneous rocks have not kept pace with the geochemical advances (e.g. Jerram and Davidson, 2007). It seems obvious that we can not successfully interpret the

wealth of isotopic and trace elemental information stored in crystals if we ignore crystallization and recrystallization dynamics.

Crystal sizes and size distributions of magmatic minerals can provide important insights into the conditions in magma chambers during crystal growth and dissolution. It has been long known that CSDs of crystals appearing on the liquidus in basic to intermediate volcanic rocks either as a result of cooling in lava lakes and flows, or degassing in conduits, often have exponential shapes with increasing densities at smaller sizes (Cashman and Marsh 1988; Mock et al., 2003) [see Fig. 1a].

Contrary to the basic rocks, crystal size distributions in many silicic rocks, especially from large magma bodies exhibit concave-down distributions with a deficiency or lack of smaller crystals (see Fig. 1a). Bindeman (2003) and Gualda et al. (2004), Gualda (2006) documented this for zircon and quartz phenocrysts in pumice, extracted and imaged in three-dimensions by a variety of techniques. Zircon, an important accessory mineral in the most silicic igneous rocks has long been known to possess concave-down CSD in volcanic and plutonic rocks (Poldervaart, 1956; Bindeman, 2003). If developed from exponential CSD, these abundant concave-down CSD in silicic rocks may point to the importance of dissolution–reprecipitation processes

* Corresponding author. Tel.: +7 496 52 49687; fax: +7 496 52 44425.

E-mail addresses: simakin@iem.ac.ru (A.G. Simakin), bindeman@uoregon.edu (I.N. Bindeman).

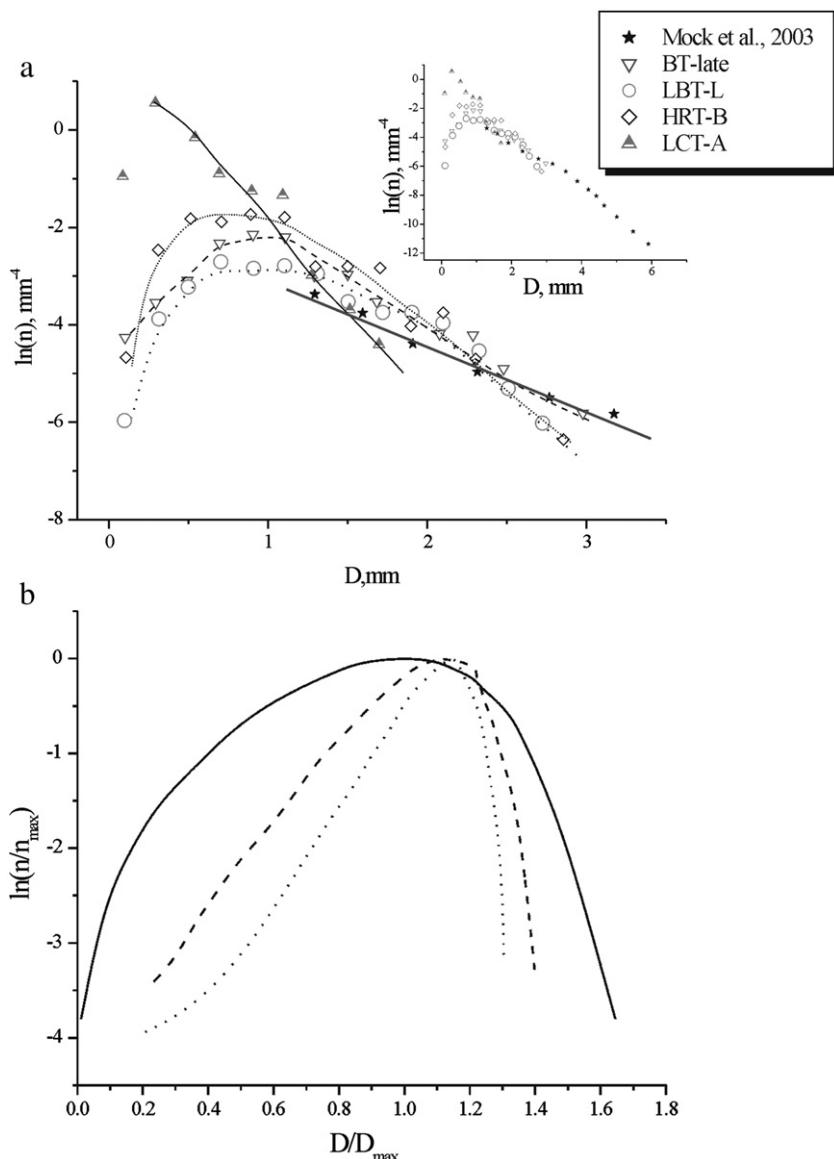


Fig. 1. Examples of the crystal size distributions in nature and experiments. a) Measured crystal size distributions of quartz in individual pumice clasts in silicic igneous rocks. Products of major caldera-forming eruptions: BT – Bishop tuff, LBT – Lower Bandelier tuff, HRT – Huckleberry Ridge tuff, LCT – Lava Creek tuff, data are from Bindeman (2003). Plutonic example is for shallow rhyolitic laccolith data is from Mock et al. (2003); crystals smaller than 1 mm size were not measured due to technique used. Quartz crystals from the volcanic rocks have smaller sizes and volume abundance and are characterized by lognormal CSDs b) Distributions normalized to the maximum crystal size and maximum abundance calculated in accordance with Slyozov–Lifshits–Wagner theory of Ostwald ripening (from Ayers et al., 2003). Three ripening mechanisms are portrayed: continuous line: controlled by interface kinetics, dotted line: by volume diffusion, dashed line: by grain boundary diffusion. Notice that Ostwald ripening processes are skewed to the right while natural CSD in (a) are skewed to the left.

or annealing. However no simple theory has explained the origin of the lognormal-like CSD (see Eberl et al., 2002 and Higgins, 2006 for discussion).

Several processes are capable of producing concave-down (log-normal) CSDs in magmatic systems, most common of which is ripening following growth (Cashman and Ferry, 1988; Higgins, 1998, 2006). Size dependent growth with growth rate increasing with crystal size has also been hypothesized to be applicable to magmatic systems, and was demonstrated in experiments of calcite growth according to the “law of proportionate effects” (Kile and Eberl, 2003). Low-intensity crystal fragmentation and dissolution of smaller fragments may lead to lognormal CSD (e.g., Kolmogorov, 1941; Bindeman, 2005), and crystal fragmentation is an important component of particle dynamics of many magmatic systems.

This paper provides description and solution of possibly the most general and common of these processes – ripening of the crystal population in the oscillating temperature regime that affects small and

large crystals differently, and, as we demonstrate below, is capable of generating the concave-down CSDs. We concentrate below on quartz and zircon, common major and accessory minerals in silicic igneous rocks. We demonstrate that several cycles of solution–reprecipitation in oscillating temperature (solubility) regime, that recycles 10–40% of crystal mass is sufficient to explain natural data and processes in magma bodies.

1.1. Theories of ripening processes

Ripening, or increase of the larger crystals at the expense of the smallest ones, is based on the size effect on solubility as was first demonstrated by Ostwald in 1896. This ripening process makes CSD plot concave-downward with left side truncation (Fig. 1b), i.e. lack of the smallest crystals. However, it has been demonstrated in experiments with silicic melts that this effect is only applicable in the smallest crystal size range of ripening of crystals $\leq 1\text{--}5\mu\text{m}$ in size

(Cabane et al., 2001, 2005). It would take 10^5 – 10^9 years (Nemchin et al., 2001) to affect larger crystal sizes because the Ostwald ripening process mostly affects crystals comparable in size to the critical nucleus of a crystal in the melt.

The general and quantitative theory of Ostwald ripening was developed by Lifshits–Slyozov–Wagner (LSW), (e.g., Lifshitz and Slyozov, 1961). According to this theory, crystals larger than some critical size grow while smaller crystals dissolve resulting in CSD with asymptotic shape, skewed to the right (Fig. 1b). The LSW theory is based on the following assumptions: 1) diffusion process of nutrients through the melt is described as the steady-state approximation for diluted suspension; 2) the surface concentration is defined by crystal size, and 3) the distant content of the dissolving component common for all particles is calculated in accordance with global mass balance that accounts for sinks (growing crystals) and sources (dissolving crystals). It follows from the LSW theory and is observed in experiments with zircons (e.g., Ayers et al., 2003) that a preexisting CSD will evolve into a different one due to the growth of larger crystals at the expense of smaller ones, yielding concave-down at small sizes CSD.

In accordance with LSW theory, time evolution of CSD by Ostwald ripening leads to the asymptotic distribution (e.g. curves in Fig. 1b) and the number of crystals depends asymptotically on time as $1/t$ and the average crystal size \bar{R} as $t^{0.5+0.333}$. The asymptotic dependence, among other things, means that CSD becomes this asymptotic function $F(\zeta)$ of the similarity variable $\zeta = R/t^n$, with time; it just shifts to the larger sizes keeping its skewed to the right shape, that is quite different from natural CSDs skewed to the left.

Recently the LSW theory was developed further with inclusion of the distribution of growing and dissolving crystals in space (Communicating Neighbors Theory – CN) and correspondent complex diffusion field (Higgins, 1998). In all these ripening models, maturation of the crystal population is considered in a static temperature field and involving long geologic times. Furthermore, while these ripening theories are applicable to mafic magmas with low viscosities and higher diffusivities of nutrient elements, and higher growth rates of crystals, it is doubtful that crystal ripening in the size range up to 100 μ m to several mm would happen in silicic magmas at realistic geologic time (e.g. Cabane et al., 2001, 2005).

In this paper, we suggest that the dissolution–precipitation processes of crystals in silicic or more basic systems are driven by the external temperature oscillations that are inherently and inevitably present in natural magma chambers. Any realistic magma system is characterized by temperature oscillations with amplitude larger than Ostwald's driving force – characteristic effective superheating for common crystal sizes. We consider examples of ripening of quartz and zircon in large volume rhyolites and demonstrate that rather large, tens of degrees temperature oscillations recycling tens of percent of crystal mass is a preferred explanation for their CSDs. We briefly discuss implications for the processes in several large magma bodies parental to Yellowstone and Bishop tuff caldera-forming eruptions.

1.2. Size effect of solubility on examples of quartz and zircon

Crystal sizes in any magmatic system vary from < 1 μ m to the microscopic scale. The contribution of the interface energy to the bulk thermodynamic properties is more important for the smaller crystals. This crystal size effect gives rise to the notion of the critical size during nucleation, which needs to be exceeded for thermodynamically stable phase transition to occur. This critical size is equally applicable to the nucleation of bubbles or crystals in the melt or for the formation of the center of growth on the flat crystal face. When we consider a melt as a solvent for the crystallizing phase, crystal solubility depends on the crystal size. Crystal solubility (S) can be expressed through the surface energy of the crystal/melt interface (e.g., Lasaga, 1998), the effective

radius R (in spherical approximation) and equilibrium macro-solubility (S_0) of the sufficiently large crystals or formally at $R = \infty$:

$$\ln(S/S_0) = \frac{2\gamma\Omega}{RT} \quad (1)$$

where γ – surface energy (J/m²), T is absolute temperature, R is radius of curvature (m), Ω is molar volume of dissolved phase (m³/mol), R is gas constant (J/mol/K). It can be demonstrated (see Cabane et al., 2005, for details) that the size effect on solubility equals to the onset of the effective superheating for the smaller crystals that has an order:

$$\Delta T_{\text{eff}} = \frac{2\gamma T_m}{R\Delta H_m\rho} \quad (2)$$

here ρ denotes the density of a crystal (kg/m³), ΔH_m is melting enthalpy (J/kg), T_m stands for the melting temperature, ΔT_{eff} is in K. Calculated effective superheating as a function of the crystal radius and energy of the melt/solid interface for quartz and zircon is shown in Fig. 2. Surface energy γ is the least constrained parameter in Eqs. (1) and (2)). At the numerical modeling of the Ostwald ripening of zircon

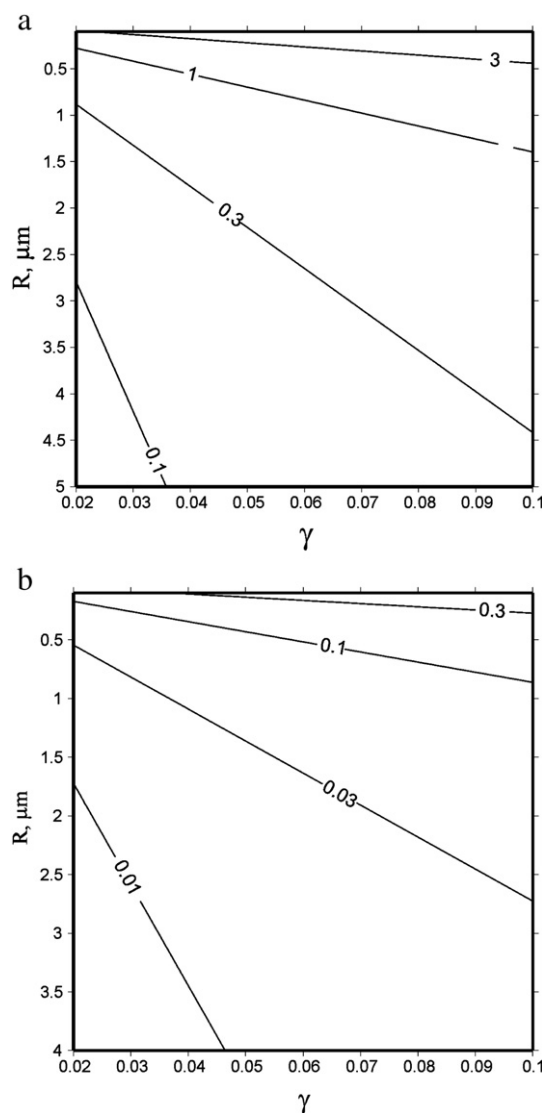


Fig. 2. Crystal size solubility effect in degree Celsius of a small crystal of spherical shape as effective superheating relative to the equilibrium flat crystal face (see Eq. (2)); energy of the crystal–melt interface γ is measured in J/m². a) for quartz b) for zircon.

in migmatites Nemchin et al. (2001) used values of γ in the range of 0.1–0.3J/m², while Cabane et al. (2005) used $\gamma = 0.5\text{J/m}^2$ for their estimates of Ostwald ripening parameters for quartz. However, one could expect that energy of the crystal phase/granitic melt is lower than the surface energy of the fluid bubbles/melt interface of 0.1J/m² in hydrous rhyolitic melt (Mourtada-Bonnefoi and Laporte, 2004) due to the lower density and structural contrast between a crystal and a melt phases. Therefore, we vary γ in the range 0.02–0.1J/m² as estimated experimentally by Hammer, (2004) for solid phases nucleated from the hydrous granitic melt. As it follows from Eq. (1) effective superheating is proportional to γ so that its estimate may vary almost on the order of magnitude due to uncertainty in the value of the surface energy. Other parameters in Eq. (2) are well known. Zircon has high density of 4650kg/m³ and dissolution enthalpy $\Delta H_m = 584.1\text{kJ/kg}$ (estimated based on the temperature dependence of solubility from Watson and Harrison, 1983). Because parameters in the denominator typically have the large values, Eq. (2) indicates a rather small effective superheating, of no more than 0.1–0.3°C, for crystals that are in the submicron size range. Quartz, on the other hand, is less dense ($\rho = 2500\text{kg/m}^3$) and has lower $\Delta H_m = 63.6\text{kJ/kg}$ (Jackson et al., 1967). As a result, driving force of Ostwald ripening during effective superheating is larger, 1–3°C at submicron sizes. Therefore we observe that the above mentioned physical properties may lead to variable intensity of maturation of different minerals.

1.3. A “realistic” magma system

In the most magma bodies there are significant to moderate variations in crystal super- and undersaturations caused by a number of factors such as temperature fluctuations, volatile driven undersaturations, and release of the latent heat of crystallization (e.g., Hort, 1998; Blundy et al., 2006). These fluctuations will variably affect different crystal sizes of different minerals. In this paper we postulate that conditions for oscillating super and under saturations are invariably present in any magmatic system. In our treatment below we describe these conditions as being driven by temperature fluctuations; this is done for simplicity and similar results would follow if equivalent super and undersaturations were caused by oscillating volatile regime, for example (e.g., Simakin and Botcharnikov, 2001).

It seems obvious that there are oscillations of temperature due to the thermal and compositional convection in magma chambers, even if in thermally-insulated magma bodies (mushy or liquid), these variations may be as little as several degrees (e.g., Marsh, 1989; Brandeis and Marsh, 1989). Temperature variations could be much larger for magmas upon ascent. Even larger amplitude temperature fluctuations are expected due to heating by fresh hot magma influxes. Such periodic temperature increases and decreases would affect saturation conditions which, in turn, will influence the evolution of the CSD of resident crystals suspended in a magma body.

Let's consider a process consisting of dissolution and precipitation stages. Dissolution may be caused by the influx of the fresh hotter magma of the same composition or by underplating of a magma chamber with the denser and hotter fresh magma. Depending on a particular temperature-composition diagram, a certain amount of heat supplied, will result in different amount of the temperature increase. For example, a near-eutectic silicic compositions will suffer much smaller temperature increase, and near-isothermal melting can take place. Nonetheless, major and accessory minerals, such as zircon, would dissolve due to dilution by melted cotectic or eutectic minerals assemblage in this case, followed by crystallization upon cooling /heat removal. This sequence of the dissolution/precipitation events is often reflected in CSD as suggested in Higgins and Roberge (2003), and is reflected in the internal structure of magmatic minerals revealed by CL or trace elemental imaging (e.g. Hoskin Schaltegger, 2003; Wark and Watson 2006; Wark et al., 2007).

Cooling is expected to be more prolonged than episode of heating, because dissipation of heat happens through the chamber walls. We should note however that hydrothermal refrigeration is a major component of many meteoric magma systems. If magma parcels that underwent superheating get surrounded by circulating hydrothermal fluids, then cooling may happen quite rapidly, sometimes leading to hydrothermal quench. However hydrothermal quench happens on the contact and quenched material will insulate main volume of magma.

We further suggest that temperature fluctuations may characterize many “experimental” magma systems. Small temperature fluctuations (and thus dissolution–reprecipitation) are unavoidable in experiments of long durations. In experiments temperature is kept approximately constant by regulators that cause oscillations around the desired value by manipulation with heating elements. However, it is known by many experimentalists that in the Internally Heated Pressure Vessels amplitude of oscillations can be several degrees depending on the design of apparatus (e.g., Eurotherm <http://www.eurotherm.com/products/controllers>).

It can be suggested, therefore, that a magma chamber, natural or experimental, is characterized by temperature fluctuations as a rule and not as an exception and thus conditions of super and under saturation, or the driving forces for recrystallization, are expected to be larger than those caused by isothermal differences in surface energy between crystal of different sizes, i.e. Ostwald ripening forces.

In the following discussion, we describe the evolution of crystal sizes in the series of the dissolution and growth events. We demonstrate that calculated dependence of the averaged CSD parameters (such as mean crystal size, volume content of crystals) from time correlate well with published experimental data.

2. Model

2.1. General formulation of the model

In general form, equation for CSD for the set of the growing and/or dissolving crystals in the heterogeneous magma can be written as (e.g., Marsh, 1998),

$$\frac{\partial n(t, R)}{\partial t} + \frac{\partial(nV(\Delta T, R))}{\partial R} = 0 \quad (3)$$

where $n(R, t)$ is a population density of crystals per 1m³ of melt, V is a growth rate in m/s, and R is a crystal radius. Crystals are assumed spherical for simplicity. This equation neglects the sedimentation process that would additionally affect particle dynamics of crystallizing systems, because small crystals do not settle much in viscous rhyolitic magmas given model timescales considered in this work.

Boundary condition describes formation of the new crystals with the size $R = 0$ in the moment t . The crystal size density at $R = 0$ is a ratio of the nucleation rate $J(t)$ to the growth rate $V(t)$, since the faster the growth rate, the faster crystals gain larger size and leave the smallest bin class:

$$n(R = 0, t) = J(t)/V(t) \quad (4)$$

For a particular case when nucleation rate $J(t) = 0$, crystal density function $n(R = 0, t) = 0$; The homogeneous nucleation rate $J(t)$ strongly depends on the driving force of crystallization as $\exp(-a/\Delta T^2)$ (Tammann, 1898), which could be expressed as undercooling, supersaturation, or Gibbs potential difference (e.g., Hammer, 2004). Such strong dependence on the degree of undercooling leads to a threshold undercooling of minimum 25–50°C for silicic magmas (James, 1985; Hammer, 2004) for homogeneous volume nucleation to start. Next, expansion of Eq. (3) yields the following expression with rates of growth and dissolution $V(R)$ being, in a general case, a certain function of the crystal size:

$$\frac{\partial n}{\partial t} + V(R) \frac{\partial n}{\partial R} + n \frac{\partial V(R)}{\partial R} = 0 \quad (5)$$

Obviously, for the rate of growth that is independent of crystal size, the last term is equals to 0, and the remaining equation is the population balance equation as defined by Marsh (1988, 1998).

2.2. Method of solution

Eq. (5) is hyperbolic and can be solved on the characteristics in closed-form. Method of characteristics consists in the reducing Partial Differential Equations (PDE) to Ordinary Differential Equations (ODE) – on some curves in the solution space. This method is widely used in the solution of hyperbolic PDE of gasdynamics (Scott, 2003). Characteristics of Eq. (5) are curves in (R,t) space defined by $dR/dt = V(R)$ (see Fig. 3). The $V(R)$, velocity of crystal growth or dissolution, is a variable quantity that depends on crystal size. In other words these are trajectories of the crystals growing with rate $V(R)$, on which PDE (5) is reduced to ODE describing variation of the distribution density for crystals with initial size $R(0) = R_0$

$$\frac{dn}{dt} + n \frac{dV(R(t))}{dR} = 0, \quad (6)$$

where time derivate now is in Lagrangian coordinates (moving with particle coordinate frame). It is obvious that when the growth rate does not depend on the crystal size, trajectories of individual crystals are parallel so that CSD function is translated from the smaller to the larger sizes along trajectories. If trajectories diverge, the density function drops and vice versa. In Fig. 3 crystals grow in time with growth rate being a function of size reaching a maximum at some crystal radius $R = R_{max}$. Crystals with sizes less than R_{max} start growing with $dV/dR > 0$; their trajectories diverge in (R,t) space and distribution density of their CSD drops in accordance with Eq. (6). After R_{max} is reached, the dependence of growth rate on size changes sign $dV/dR < 0$, trajectories start converging, and a number of crystals n starts to rise. Crystals with initial sizes above R_{max} move by converging trajectories from the initial moment. In our artificial example CSD with maximum will form from the initially uniform distribution. We consider implication of this below.

2.3. CSD solution for sequence of dissolution and growth events

Here, we describe CSD evolution for a preexisting crystal population with an initially exponential CSD (Fig. 1b), similar to ones found in many igneous systems (e.g. Cashman and Marsh, 1988), when there are small fluctuations of growth/dissolution driving force (e.g., temperature) around a relatively constant temperature. Given relatively large undercooling required for new volume homogeneous nucleation to

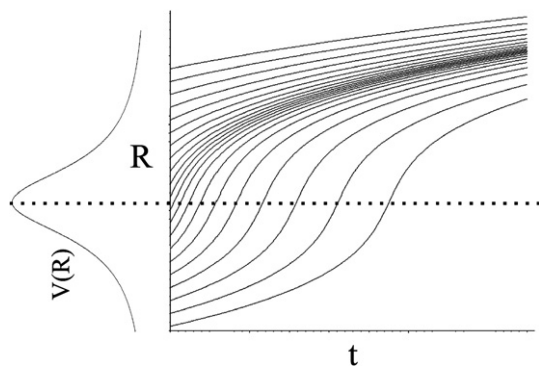


Fig. 3. General view of growing crystal trajectories in (R,t) space plotted to illustrate how method of characteristics works in CSD case. An abstract dependence of growth rate on the crystal radius $V(R)$ with maximum at some $R=R_{max}$ is taken. For reference it is plotted along with R axis. Trajectories of the sample crystals in (R,t) space deviate at $dV/dR > 0$ for $R < R_{max}$ providing decrease of the CSD population density function. In the region where $dV/dR < 0$ trajectories of crystals are crowded providing growth of CSD density.

start in silicic magmas (see above and James, 1985; Hammer, 2004), we assume that new homogenous nucleation does not happen at small temperature fluctuations, but instead these systems are characterized by heterogeneous nucleation, or growth of the existing and surviving larger crystals. Let's consider dissolution and growth stages.

2.3.1. Dissolution stage

During the initial melt fraction or the temperature increase, the dissolution rate of a particular crystal is taken to be inversely proportional to its size. This happens due to dependence of the diffusion flux from curvature of the dissolving crystal surface (see Appendix A for details):

$$V = -a(t)/R \text{ or } dV/dR = a(t)/R^2 \quad (7)$$

$$a = D(C_b - C_0)\rho_l / (C_s - C_0)\rho_s \quad (7a)$$

where V is the dissolution rate, D is the diffusion coefficient of the slowest diffusing component that comprises dissolving solid in the melt, and a is the constant proportional to the degree of undersaturation $(C_b - C_0)$, where C_b is solubility of the slowest diffusing component in the melt or its concentration on the crystal boundary, C_0 is content of this component in the melt away from the boundary, C_s is component content in the solid. Diffusive crystal dissolution is primarily rate-limited by the diffusion of the slowest component in melt (Zhang et al., 1989). Hence, the radius of crystal is getting reduced with time as a square root of time:

$$R = \sqrt{R_0^2 - 2Ja(t)t} \quad (8)$$

Generally, crystal size density $n(R,t)$ depends both on the crystal radius R and time t . On the characteristics, density n depends on time, while the radius is also a known function of time (see Eq. (3)). Substituting dependence $R(t)$ on the characteristics Eq. (8) into (6) using Eq. (7) yields the following solution:

$$n(R, t) = n_0(R_0, t=0) \frac{R(R_0, t)}{R_0(R, t)} \quad (9)$$

Here the radius R (in the moment of time t) corresponds to some larger radius R_0 in the initial moment of the dissolution event.

Alternatively we can express the initial size R_0 corresponding to the current R as function of time and insert into Eq. (9) to get

$$f_{1/2} = n(R, T) = n_0 \left(\sqrt{R^2 + c} \right) \frac{R}{\sqrt{R^2 + c}}, \quad (10)$$

where $f_{1/2}$ designates the distribution corresponding to the first stage of the dissolution-growth cycle and coefficient $c = 2at = 2D(T)(C_b - C_0)\rho_l t / \rho_s(C_s - C_0)$ at the approximately constant undersaturation and diffusion coefficient. When some linear scale for crystal size R_0 is set, coefficient c gets non-dimensional form $c = 2D(T)(C_b - C_0)\rho_l t / \rho_s(C_s - C_0)R_0^2$.

2.3.2. Overgrowth stage

Generally at slow conductive cooling that is controlled by the heat loss into country rocks, crystallization would proceed in the regime controlled by the kinetics of slow crystal growth rather than be rate-limited by diffusion through the melt (Lasaga, 1998; Hort, 1998). On the contrary, upon fast cooling, crystal growth is controlled by diffusion towards the growing crystal faces, edges, and vertices. Dendrites and hopper morphology crystals are attributes of this diffusion control (e.g., Donaldson, 1976 for olivine; Simakin and Chevychelov, 1995 for feldspar), since elongated, and narrower crystals grow faster due to enhanced diffusion transport at their tips (e.g., Lofgren, 1980). At the interface-controlled growth, perfectly-faceted crystals develop and

the larger crystals tend to grow faster. It can be caused by requirements of the spiral growth mechanism that needs crystal faces that are extended enough (e.g., Lasaga, 1998). Spiral parameters depends on the supersaturation, spirals at the growth of magmatic minerals sometimes have surprisingly high step height (much more than the several atomic layer sizes) (Sunagawa, 1984). There are reasons why larger crystals would grow faster in a kinetic regime (e.g., growth rate is proportional to the number of the growth spirals on the flat face). However, there are convincing examples of the growth rate being independent on the crystal size, as is demonstrated by the slow overgrowth of garnet in metamorphic conditions using 3D imaging and analysis by Cheng et al. (2008). Here for simplicity in the solution we will use growth rate not dependent on the crystal size. Then, at the growth stage, all crystals would gain increment in their size $\delta R = \int v dt$. Density of crystal size distribution at such process is shifted to a larger size without shape distortion so that its value corresponds to the values at the end of dissolution stage $n(R - \delta R)$. Combining growth and dissolution stage (Eq. (10)) we get a recursive relation between CSD after one dissolution-growth step:

$$n_k = \frac{n_{k-1} \left(\sqrt{(R - \delta R_k)^2 + c_k} \right) (R - \delta R_k)}{\sqrt{(R - \delta R_k)^2 + c_k}} \quad (11)$$

where parameter c is defined above (see Eq. (10)) relates to the amount of dissolved material and does not depend on the crystal radius.

At two dissolution/precipitation events the initially exponential distribution $n_0 \exp(-\gamma R)$ becomes:

$$n_2 = n_0 \frac{\exp \left(-\gamma \sqrt{\left(\sqrt{(R - \delta R_{1+2})^2 + c_1 - \delta R_2} \right)^2 + c_2} \right) \left(\sqrt{(R - \delta R_{1+2})^2 + c_1 - \delta R_2} \right)}{\sqrt{\left(\sqrt{(R - \delta R_{1+2})^2 + c_1 - \delta R_2} \right)^2 + c_2}} \quad (12)$$

Calculations at number of events $k > 2$ are tedious and were performed with symbolic manipulator Maple (http://en.wikipedia.org/wiki/Maple_computer_algebra_system).

Two distinct regimes of recrystallization can be recognized. These two cases represent two likely end-members during magma convection and temperature change.

- 1) Equilibrium. Total amount of the dissolved material $dM_{\text{dissolved}}$, can be set as some fraction of the initial mass of crystals before dissolution, $dM_{\text{dissol}}/M_0 = \text{const}$. At the end of dissolution stage, the equilibrium saturation level is attained for the final temperature. This case applies when duration of the heating event is larger than time necessary to achieve equilibrium at dissolution. Equilibrium dissolution time is approximately proportional to c_k , the variable that depends on the current CSD parameters.
- 2) Non-equilibrium. Amount of the dissolved material is proportional to time during the dissolution stage or $c_k = \text{const}$, and is only a fraction of the equilibrium dM_{dissol} . This case applies when the time between temperature fluctuations is short, and slow kinetics prevents the required equilibrium mass to be dissolved during each dissolution episode to achieve saturation level, and then dissolution is forced to stop (quenched) at the subsequent cooling stage.

In these two cases, the small increment of crystal size change δR during each step of precipitation (δR_k) is calculated to keep crystals mass balance constant and identical to the initial crystal mass as defined by the initial CSD. In other words, the mass of all crystals at the end of each precipitation episode equals the initial mass M_0 .

In order to calculate the parameter c_k in k the equilibrium dissolution step (Case 1), and the parameter δR_k , we solve numerically equations involving the mass of the crystals for a given size distribution

$$M_k = \int_{R_{\text{min}}}^{R_{\text{max}}} 4/3\pi R^3 n_k dR \quad (13)$$

The minimum crystal size for the initial exponential CSD is set to zero. After the first growth step, the minimum size becomes δR_1 . During the next steps R_{min} and δR_k are calculated in accordance with the amount of the dissolved and reprecipitated material for each initial CSD and crystal mass. An example of the evolution of a sequence of the calculated CSDs is shown in Fig. 4a. It is evident that maximum of the distribution is shifted to the larger sizes and becomes wider with increasing number of the dissolution-precipitation cycles. Initial steepness of the starting exponential CSD affects evolution of the CSD shape. This effect is illustrated in Fig. 4b depicting evolution of three initially different CSDs in which crystals volume content is 0.3; these CSDs are subjected to the equal sequence of three dissolution-precipitation events each recycling 30% of the crystal mass. It can be

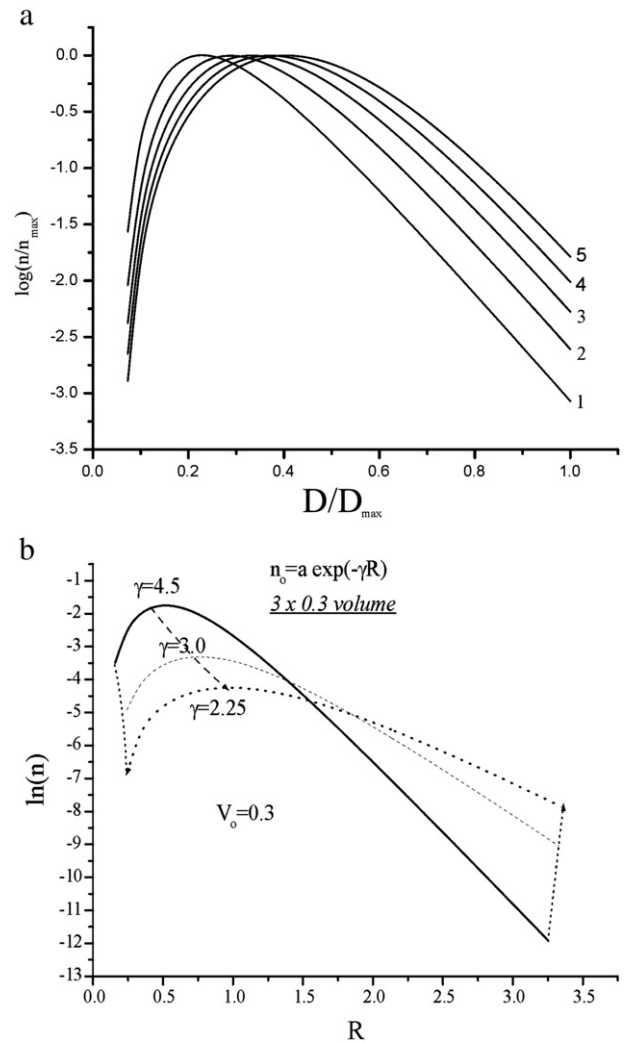


Fig. 4. An example of the calculated CSDs after several dissolution/precipitation steps. a) evolution of CSD in series of five steps, in each step 0.25 of the crystals volume is dissolved and reprecipitated, while crystal mass is conserved: lowering of the maximum value of the CSD is compensated by its overall shift to the larger mean crystal size values. At each cycle of re-precipitation of 25% of crystal mass, parameter c_k gets different values. Notice that shapes of distributions are similar to natural ones (Fig. 1a). b) series of CSDs with different initial exponential distributions $n(R) = n_0 \exp(-\gamma R)$. In all cases crystals comprise 0.3 of volume and matured in the course of three cycles reprecipitating 0.3 of crystal mass.

seen that if the initial distribution has greater fraction of the smallest crystals, the resultant CSD will have narrow maximum at the smallest size on the CSD plots. The larger size shoulder of CSDs changes initial slope only when maximum is sufficiently shifted and widen.

2.3.2.1. The potential role of size dependent growth caused by crystal settling. If growth rate is proportional to the crystal size (e.g., Eberl et al., 2002) then it may lead to somewhat faster growth of larger the crystals while minimally affecting the smallest crystal sizes that are undergoing dissolution. In natural systems, diffusive mass transport can be accelerated due to Stokes crystal settling. The larger crystals sink faster and have narrower boundary layer that facilitates diffusion of the dissolving components from their crystal surface. This effect can be quantified with scaling relationships obtained experimentally and theoretically decades ago (Bowman et al., 1961; Brauer and Schmidt-Traub, 1973). In Fig. 5 our estimates for quartz and zircon (see Appendix B for details) are displayed demonstrating that in the granite melt, diffusive flux and dissolution rate are inversely proportional to the crystal radius until some threshold value that primarily depends on the density of settling crystals. For a crystal settling in the granite with viscosity of 10^5 Pa s, the effect of accelerated dissolution caused by crystal settling starts playing a role for zircon crystals larger than $20\mu\text{m}$ in radius, for the less dense quartz crystals this radius is about 0.5mm . For crystals greater than the quoted sizes, effect of accelerating of the relative flow due to increase of R merely compensates decrease in the diffusive flow for increasing curvature so that dissolution rate becomes almost constant. Therefore, we neglect the effect of flow in our model, because most dissolution/precipitation ripening happen at sizes smaller than the quoted sizes.

3. Applications of the model

3.1. Experimental coarsening

We start with consideration of experimental data on the coarsening of the fine crystals suspension in the melt by dissolution-precipitation mechanism in order to see if these can be explained by oscillating temperatures. Crashing of the mineral grains with mortar

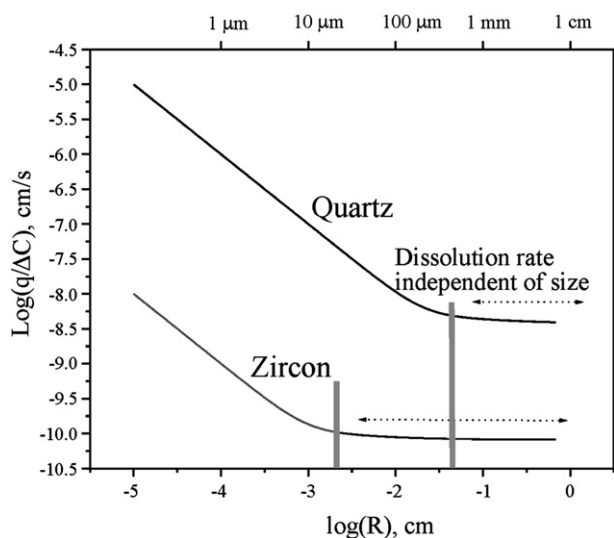


Fig. 5. Dependence of the total mass flux (q) from the surface of the sphere moving with constant velocity through the viscous liquid calculated in accordance with a model of Brauer and Schmidt-Traub (1973). Constant concentration on the sphere surface C_b is set, flux (in $\text{cm}^3/\text{s} = \text{cm}^3/\text{cm}^2/\text{s}$) is normalized on the $\Delta C = C_b - C_\infty$. Stokes settling velocities for quartz and zircon in the granite melt with viscosity 10^5 poise are used, with densities of quartz at 2650 kg/m^3 , and zircon at 4800 kg/m^3 . Notice that at given parameters for zircon crystal sizes ($2R$) > ca $40\text{--}50 \mu\text{m}$ and quartz greater than about $0.4\text{--}0.5 \text{ mm}$ dissolution is independent on settling rate.

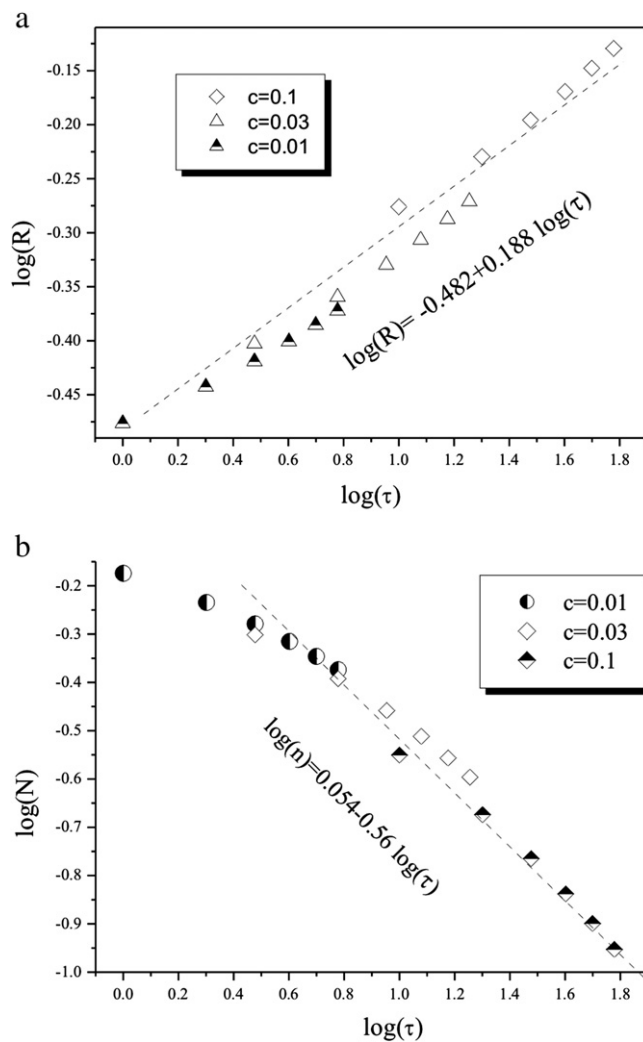


Fig. 6. Dependence of the mean crystal radius (a) and the volume number content (b) on time in the series of five small amplitude dissolution-precipitation events. Time (t) is set approximately proportional to the number of cycles (n) multiplied on the non-dimensional rate parameter c in Eq. (10) ($T = 100cn$). Parameter c is proportional to dissolution time at constant superheating. Parameter $c = 0.1$ on the plot corresponds to the oscillations with the largest period. Notice that there is no difference in the end result on whether the dissolutions were small in number but intense or if there were large number of smaller-degree dissolutions.

and pestle prior to experiments may yield exponential CSD (Djamarani and Clark, 1997), fractal or Weibull CSDs, with subtly concave-down shape in semi-logarithmic coordinates (e.g. Bindeman, 2005), all having plentiful small crystals. When for example an exponential CSD is allowed to anneal in experiments involving a melt or fluid, it develops concave up, lognormal CSD as is observed in experiments with duration from day to weeks on fluid driven metamorphic zircon maturation affecting zircon crystals in the size range $0.1 < R < 2\mu\text{m}$ (e.g. Ayers et al., 2003). We suggest that the annealing and CSD transformation in experiments may be better explained by temperature fluctuations rather than by Ostwald ripening, because of the reasons outlined above and below.

The effect of the particle size on solubility (driving force for Ostwald ripening) can be expressed in terms of effective superheating in degrees of Celsius relative to a flat crystal face of a given mineral in equilibrium with melt (see Eqs. (1) and (2)). It can be calculated to be about one degree for quartz and 0.1°C for zircon in the granitic melt based on the Eq. (2) above. Therefore crystals with radius of several microns and more will recrystallize faster at the temperature oscillations with amplitude of several degrees in experimental systems than at the classic isothermal Ostwald ripening.

Temperature fluctuations on the order of 1–5°C are typical among many temperature controllers for the furnaces such as Eurotherm and others, and thus all nominally isothermal experiments are getting affected.

We model the temperature fluctuation process by using small values of parameter c (0.1–0.01) and applying up to 7 steps of solution–reprecipitation to the initially exponential distribution. Fig. 6a presents results of calculations of the evolution of the average crystal radius (first moment of CSD function) for different values of c . It is important to stress that, the average slope of the dependence in bi-logarithmic coordinates in Fig. 6 is about 0.19. Due to the dissolution of the small crystals total number of crystals in the unit volume N continuously decreases with time. Correspondent slope of dependence N versus time in bi-logarithmic coordinates is 0.56 (see Fig. 6b). On the later stage relationship $N * \bar{R}^3 = \text{const}$ following from the mass balance, holds, where mean radius $\bar{R} = \int_0^{\bar{R}^{\text{max}}} n(R) R dR / \int_0^{\bar{R}^{\text{max}}} n(R) dR$ and $N = \int_0^{\bar{R}^{\text{max}}} n(R) dR$. It can be shown that the relationship $N * \bar{R}^3 = \text{const}$ holds in series of $n_i(R)$ when they are similar in some sense (e.g., self-similar). If formulas for $n_i(R)$ are not similar (one exponential, another lognormal) $N * \bar{R}^3_{\text{mean}}$ can vary as we see in Fig. 6b.

It is important to estimate physical timescales associated with our theoretical non-dimensional results presented above for experimental coarsening. We calculate time scales that are appropriate for quartz and zircon (see Fig. 7a and b). Time of the dissolution stage for quartz at superheating $\Delta T = 2^\circ\text{C}$ and non-dimensional parameter $c = 0.01$ was calculated with diffusion coefficient D_{SiO_2} for rhyolitic melt with water content 4wt.% varying with temperature according to Baker (1991) ($D_{\text{SiO}_2} = 3.3 \cdot 10^{-10} \text{cm}^2/\text{s}$ at $T = 800^\circ\text{C}$). However, recent study by Acosta-Vigil et al. (2006) demonstrates that SiO_2 diffusion during experimental quartz dissolution in rhyolitic melt is about one order of magnitude slower ($D_{\text{SiO}_2} = 2.0\text{--}3.0 \cdot 10^{-11} \text{cm}^2/\text{s}$ at $T = 800^\circ\text{C}$ and $P_{\text{H}_2\text{O}} = 2 \text{kbar}$) than diffusion of SiO_2 during interdiffusion of the dacite–rhyolite melt couples (Baker, 1991) or at the dissolution of alkali feldspars in the granite melt (Acosta-Vigil et al., 2006). However, Acosta-Vigil et al. (2006) presents diffusion data for a single temperature. We consider silica diffusion results of Acosta-Vigil et al. (2006) more realistic for our study, and therefore we use the D_{SiO_2} value quoted above but assumed that activation energy and temperature dependence of Baker (1991). For the temperature dependence of the solubility quartz liquidus parameters in the system Ab–Qz are taken from Johannes and Holtz (1996) to transform ΔT into ΔC . Dissolution–precipitation process is rather effective at several micron-size scale, fluctuations of about 10min order of magnitude period with amplitude 2°C will lead to the appreciable coarsening of the quartz suspension (see Fig. 7a).

Zircon is more difficult to dissolve than quartz, because diffusion coefficients through the melt are lower for zirconium and solubility with associated concentration gradients are small (e.g. Watson and Harrison 1983 vs Baker, 1991).

We calculate time scale corresponding to $c = 0.01$ and amplitude $\Delta T = 2^\circ\text{C}$ by using diffusion coefficient for Zr for rhyolitic melt with water content 4wt.% and parametrized temperature dependence of the zircon solubility from Harrison and Watson (1983). The dissolution–precipitation process on a normal experimental time scale of days is only possible for the smallest sizes, around $1\mu\text{m}$, and highest temperature (see Fig. 7b). We conclude that contribution of the thermal oscillations may dominate in the producing experimental lognormal CSD of quartz and zircon as compared to the Ostwald ripening mechanism. However we are unaware of any experiments that crystallize zircons from the melt and report their CSD.

3.2. Approach to the interpretation of the natural CSDs

While in experiments we considered small temperature fluctuations, natural examples provide the evidence of large solution–reprecipitation episodes, recycling up to 50% of crystal mass (Wark et

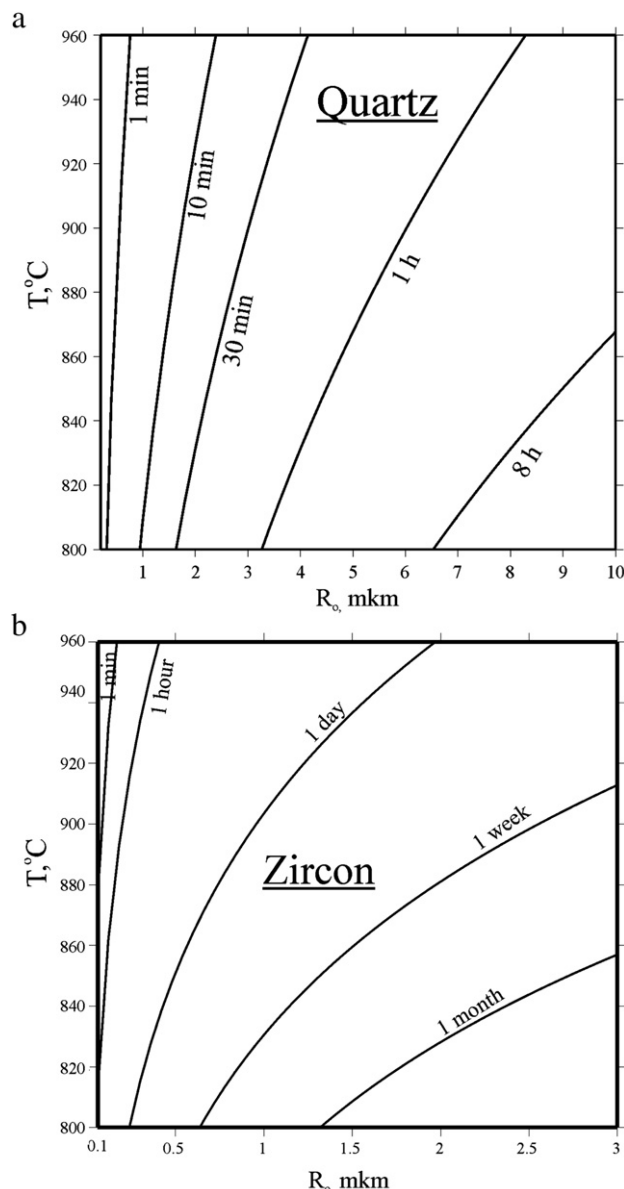


Fig. 7. Time of the dissolution stage at superheating $\Delta T = 2^\circ\text{C}$ and non-dimensional parameter $c = 0.01$ as a function of temperature and crystal size. Rhyolitic melt with water content 4 wt.% and $T = 800^\circ\text{C}$ is considered and the temperature dependence of the solubility of quartz in the system Qz–Ab taken from Johannes and Holtz (1996) as representative for a rhyolitic magma. a) for quartz. Silica diffusion coefficient are in accordance with (Acosta-Vigil et al., 2006 and Baker, 1991) for $\text{H}_2\text{O} = 4 \text{ wt.}\%$. Dissolution–precipitation process is rather effective at 1–10 μm size scale, fluctuations of the 10 min or less scale with amplitude 2°C will lead to the appreciable coarsening of the quartz crystal population smaller than 1–2 μm . b) for zircon. Diffusion coefficient for Zr for rhyolitic melt with water content 4 wt.% is used in calculations, which also accounts for parametrized temperature dependence of the zircon solubility (Harrison and Watson, 1983). Dissolution–precipitation process in a normal experimental time scale of days is only possible for the smallest sizes and highest temperature. Due to the slow zirconium diffusion, we can expect that long-duration experiments of several months may display coarsening of crystals of submicron size.

al., 2007; Bindeman et al., 2008). There is the trade-off effect between the fluctuation amplitude and the number of fluctuations to produce the desired CSD as mentioned above. Therefore our reconstruction of the number of the heating events causing crystal mass recycling and their amplitudes based on the CSDs are taken as informed prejudices (or educated guesses) on particular magma systems. An additional information like the observation of internal crystal zoning indicative

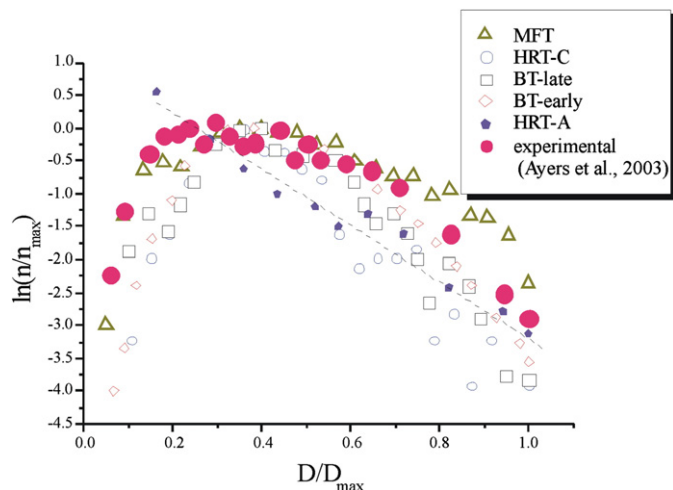


Fig. 8. Crystal size distributions for zircon extracted from pumice in large volume pyroclastic tuff deposits (data from Bindeman, 2003) normalized on the maximum crystal size and maximum CSD value. For comparison experimental data on the zircon CSD matured in the nominally isothermal hydrothermal ripening experiment within quartzite are shown (data from Ayers et al., 2003). In experiments, zircon ripening occurred presumably due to multiple, low amplitude temperature oscillations. Notice that experimental and natural CSDs are comparable, but in experiments CSD has flattened top with maximum shifted to the smaller size compared with natural distributions, see text for discussion.

of dissolution–precipitation events in individual crystals can be used to constrain the number of cycles. If independent data is available about the timing between different cycles, then a total time for crystal maturation can be estimated from a CSD.

In our applications to the natural CSD, we consider CSD of quartz and zircons in individual pumice clasts from large volume caldera-forming eruptions that were reported in Bindeman (2003). While zircon exhibits no evidence for postcrystallizational breakage, melt inclusion decrepitation is the leading cause of quartz breakage generating fractal or lognormal fragment size distributions (Bindeman, 2005). However the present work only discusses CSDs of unbroken crystal populations (Bindeman, 2003). The list of units discussed here include: Huckleberry Ridge tuff (HRT, Members A and C), Mesa Falls tuff (MFT), Lava Creek tuff (LCT, Member A and B), and Bishop tuff (BT, Early and Late). The first three tuff units were erupted in the course of 2.04, 1.3, and 0.64Ma caldera-forming eruptions of Yellowstone, while BT was a product of 0.75Ma eruption of Long Valley Caldera, California. Since zircon and quartz were rapidly quenched by eruption, the extracted populations of whole crystals and their CSD reflect quenched, pre-eruptive conditions of crystal growth and dissolution and thus may provide useful information about initiation of their respective caldera-forming eruptions. It is particularly noteworthy that CSD of quartz and zircon are lognormal in all cases, and we suggest that this is a result of the annealing of an initially exponential CSD in the course of pre-eruptive temperature spike in each pre-climactic magma chamber.

In order to compare shapes of crystal size distributions of quartz and zircon for samples of different crystal content and median size, we normalized these two parameters to the maximum density value and maximum crystal size in each sample (see set of the distributions for zircon in Fig. 8). Such procedure does not change the shape of the CSD and allows us to discuss annealing progress recorded in shape as a function of the number of solution–reprecipitation steps, n . Shapes of the CSDs differ by the width of the D/D_m size spectrum (flatness), position of the maximum (shifted to smaller or larger relative sizes), and steepness of the small size shoulder. For example, the CSD of MFT zircons have most flattened shape, while CSD for BT-Early have the steepest.

We explore what number of the relatively large amplitude temperature oscillations and correspondent dissolution–precipitation events will result in the CSD of a given shape. Exponential distribution demonstrated by zircons from HRT-A tuff is typical for as-grown crystals not subjected to recrystallization. It is reported for the magma bodies with simple thermal history such as solidified lava lakes (Cashman and Marsh, 1988), rhyolitic laccoliths (Mock et al., 2003), some intrusions (Higgins, 1998), and selected silicic eruptive products (Bindeman, 2003; Higgins and Roberge, 2003). However for the majority of other tuffs a number of episodes of temperature oscillations, and dissolution of smaller crystals is required (Figs. 8 and 9). In order to fit the natural data for each eruption, we started with the initially exponential distribution as defined by the slope of the right-hand side shoulder of the natural distribution and undertook a modeling by trial and error to obtain a best-fit solution for details of the concave-down, lognormal shape of crystals in each eruption.

We notice that only one to three episodes are sufficient to reproduce the lognormal shape, and fine-tuning of this model usually requires 1–2 additional smaller steps of dissolution rather than a

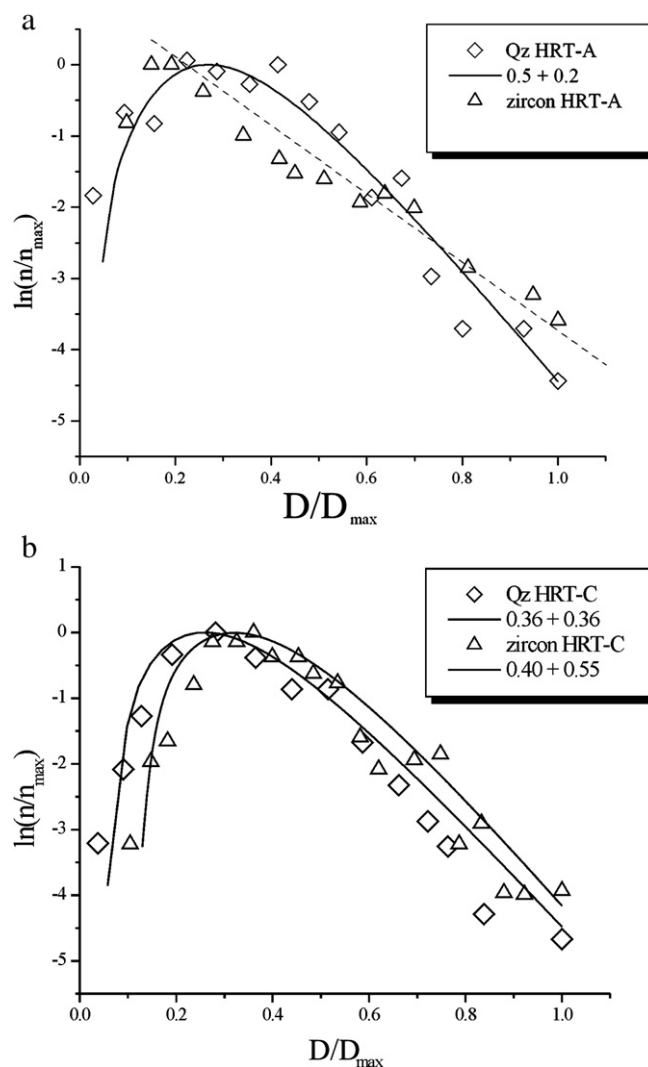


Fig. 9. Interpretation of CSDs for quartz and zircon from the Huckleberry Ridge tuff eruption of Yellowstone, Members A (a) and C (b). Model curves were fit to best describe measured values and present proportion of crystal mass recycled in each of the dissolution/precipitation cycles, while keeping the overall crystal mass the same. Notice that zircon in Member A has exponential distribution in the contrast to quartz in the same sample and requires no annealing. Quartz and zircon of the Member C can be explained by two dissolution/precipitation episodes of approximately the same magnitude. See text for discussion.

single episode that recycles a significant portion of the original crystal mass. Overall, a moderate (i.e. 10% total mass) to significant (e.g. 60%) of total crystal mass is required to be dissolved and then reprecipitated in order to explain the observed concave-down CSD shape and its details as is observed on Figs. 8 and 9. As a rule of the thumb, a single reheating–recycling episode leads to very steep truncation of the left hand CSD shoulder, than a series of smaller dissolution–reprecipitation episodes, because in the latter case there is a greater chance for smaller crystals to survive dissolution regrow between reheating episodes and thus the CSD is able to recover toward a smoother shape.

We attributed small temperature oscillations to details of magma convection in subliquidus magma bodies (e.g. Marsh, 1989), or spiked episode of latent heat released/hydrothermal refrigeration by mushy-state, near solidus magma bodies but the proportions of crystal mass recycling required to explain our natural data are more in line with rather large reheating episodes. It is known that in subvolcanic magma chambers resident silicic magma can be subjected to several reheating events by an intruding basaltic magma; such events are recorded in the mineral zoning and clearly exemplified by magma mixing textures. Therefore we consider such reheating episodes to be the main driving force of recrystallization and transformation of the initially exponential CSD into lognormal one in several dissolution–reprecipitation cycles.

However, another variation of the theme that are likely to be characteristic of natural system: is when—the temperature increases are too rapid for dissolving crystals to achieve the equilibrium dissolution fraction, before the next episode of temperature decrease causes crystal overgrowth. This corresponds to the case 2 above and may characterize recrystallization of zircon in nature. Due to the relatively faster diffusion of silica vs. zirconia in melts (Baker, 1991 and Watson and Harrison, 1983), quartz dissolution may follow the equilibrium model (i.e. case 1 above); zircon dissolution may still be incomplete when the temperature drops, and thus its dissolution may be ceased before the next episode of overgrowth. However, equilibrium or not, the final CSD will look similarly lognormal and below we present case studies from the natural examples of the same large silica rhyolites. We demonstrate that only a few, one to three, episodes are required to explain the observed natural CSD for quartz and zircon.

3.3. Quartz and zircon examples from Huckleberry Ridge tuff, Bishop tuff, and Mesa Falls tuff

We consider CSDs for both quartz and zircon in these three large volume tuffs. Products of the early stage of eruption that produced the Huckleberry Ridge tuff –Member A (Fig. 9a) are characterized by moderately matured quartz CSD with maximum at $D/D_m \approx 0.33$ that are best obtained in only two cycles of dissolution–reprecipitation episodes each recycling 0.50 and 0.20 fraction of quartz crystals by mass. However, zircon crystals in this sample demonstrates almost exponential distribution and requires little annealing: maximum is defined only by one left point on the CSD plot and distribution can be treated as practically exponential or as a result of pure grown upon cooling or degassing. Zirconium concentration is the lowest in the HRT-A compare to the other units, while this is the most silica rich sample of HRT (e.g. Bindeman et al., 2008). Therefore quartz is likely to appear before zircon and have suffered episodes of solution and reprecipitation. Zircon may suffer even larger dissolution at the strong heating preceding HRT supereruption so that there were too few survived crystals and new ones nucleate and grow just before or in the final eruption stage to yield exponential CSD.

Products of the late stage of the eruption corresponding to Huckleberry Ridge tuff – Member C (see Fig. 9b) are characterized by similarly lognormal CSDs for quartz and zircon. Their shapes can be respectively interpreted as result of the re-precipitation of the 0.36×2 for quartz crystals volume, and 0.40 and 0.55 dissolution–reprecipitation

episodes for zircon. Practically concordant behavior of quartz and zircon in HRT-C rhyolites may be interpreted that quartz and zircons shared common history in the HRT-C magma body, and be caused by two episodes of rhyolitic magma heating by basic magmas. It should be noted that in HRT-A and especially HRT-C zircons many zircon cores survived remelting and recycling and reflect ages and oxygen isotopic values of that of precursor rocks (e.g. Bindeman et al., 2008).

In contrast to HRT-A, zircon CSD in the products of the early Bishop tuff eruption looks more matured than quartz CSD from the same sample (see Fig. 10a). Modeling demonstrates that CSD of quartz would be consistent with two weak episodes of dissolution–reprecipitation recycling 0.25 and 0.12 of quartz mass to match CSD with observed parameters. However, two episodes that recycle 0.45 and 0.47 of zircon mass is required to explain zircon CSD in early BT.

At the same time, quartz and zircon in the products of the late Bishop tuff eruption have quite similar normalized CSDs (see Fig. 10b). We can match both CSDs with only two cycles of dissolution/precipitation $0.42 + 0.32$ for quartz and $0.55 + 0.55$ for zircon. Apparently the fact that zircon is more matured than quartz in the early BT can be linked to small content of zircon crystals (only 28 crystals per 1 cm^3 in Early BT vs. 37–98

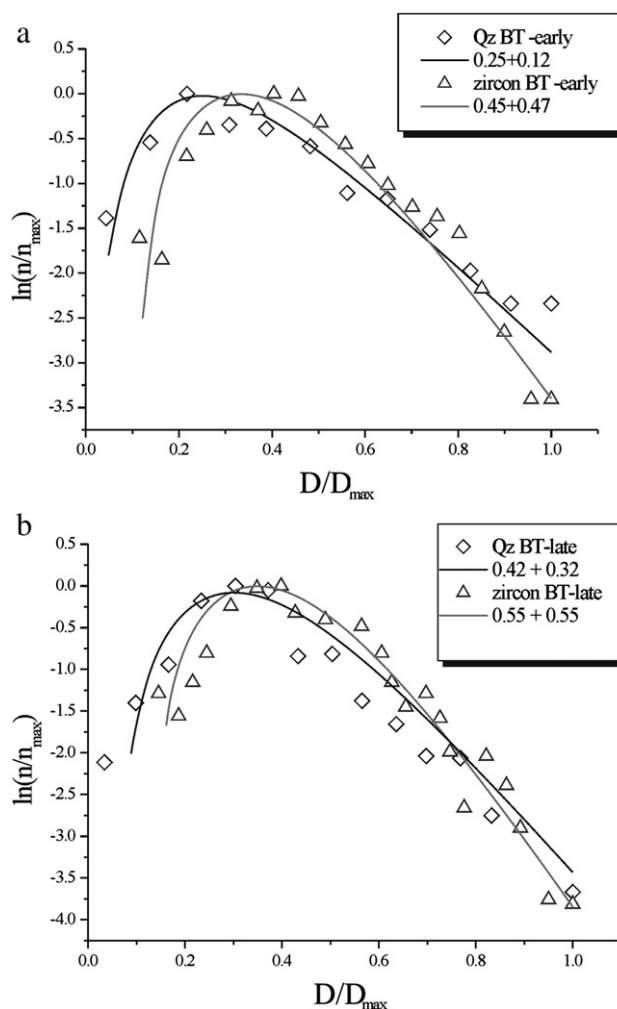


Fig. 10. Interpretation of CSDs for quartz and zircon from the Bishop tuff pumice clasts a) from early BT; b) from late BT. BT-late quartz is pronouncedly more matured than BT-early quartz in agreement with observations of the quartz cathodoluminescence and Ti concentration zonality from BT (Peppard et al., 2001; Wark et al., 2007). Zircon CSDs in early and late BT are quite similar by their normalized shape and require two episodes of dissolution/reprecipitation to match measured CSD shapes. In the Late BT, two comparable episodes of the total mass of zircon crystals per cm^3 of magma is larger. It means that less intensive melting involving quartz dissolution will act strongly on zircon CSD in BT-early as more intensive melting at higher mass of zircon crystals in BT-late).

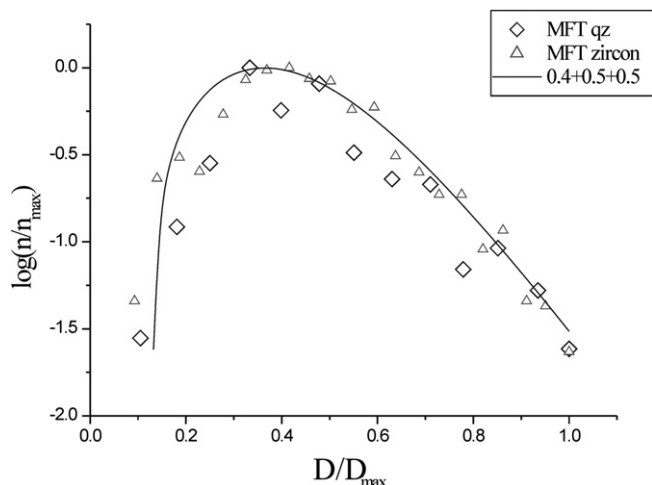


Fig. 11. Interpretation of CSDs for quartz and zircon from the Mesa Falls Tuff. Both phases demonstrate rather concordant distributions that are best interpreted as result of the three intensive solution/precipitation episodes.

crystals in late BT, Bindeman, 2003, Appendix); as a result that melting of the even small fraction of quartz would cause more substantial dissolution of zircon. Late erupted BT tuff probably represents bottom layer of magma, thermally activated due to thermal interaction with underplating basalts (e.g. Wark et al., 2007). Thermal reactivation of the deep layers in large silicic magma bodies by an underplating basic magma seems to be essential feature of voluminous rhyolitic eruptions as suggested in many studies (e.g. Annen and Sparks, 2002).

The CSDs for quartz and zircon in the Mesa Falls Tuff are most mature and demonstrate the largest crystal sizes and crystal mean sizes. They demonstrate concordant behavior of quartz and zircon in a magma stored before eruption and subjected to at least three intensive episodes of solution–reprecipitation, recycling 0.4 + 0.5 + 0.5 mass fraction (see Fig. 11). It appears that both quartz and zircons share the same dissolution–reprecipitation history in the MFT.

Examples above presented contrasting cases that may characterize recycling of two mineral phases one major and one accessory in the same rock that shows their discordant and concordant behavior. Mineral growth rates and diffusion rates of their constituent elements differ by several times and discordant behavior is expected for a non-equilibrium dissolution (case 2 above). Nonetheless, it appears that a few large scale recycling episodes are sufficient to explain our data.

3.4. Can a mature lognormal CSD tell time?

In the above calculations we controlled the number of cycles n to generate a particular CSD and made no inference on the time it takes to achieve the final (observed) CSD. Any time estimate based on the lognormal CSD will only represent a minimum residence time since a given population may reside in a large magma chamber for a long time at constant temperature or if there are only small temperature oscillations, affecting the smallest crystals. We demonstrated above that small temperature oscillations of 1–2° can explain experimental coarsening of micron-size crystals of zircon, tens to hundreds of micron crystals of zircons require much more significant oscillations of several tens of degrees C.

However if there is no idle time in each magma chamber history, and temperature oscillations come one after another, then physical time can be set proportional to product n and parameter c in Eq. (11) above since $c = 2D_{Zr}(T)(C_b - C_o)\rho_l t_{scl} / \rho_s(C_s - C_o)R_0^2$ is proportional to the time scale of dissolution stage. We plot in Fig. 6 calculated mean crystal radius as a function of $T = n \times c$ for different values of c (due to for example different period of temperature oscillations t_{scl} at constant supersaturation $C_b - C_o$).

We can estimate order of magnitude of the characteristic time of the dissolution stage based on the CSD analysis. Parameter $c = 2D_{Zr}$ or $SiO_2(T)\Delta C\rho_l t_{scl} / \rho_s(C_s - C_o)R_0^2$ controls dissolution process. For quartz parameter $\Delta C(\Delta T) = C_b(T_o + \Delta T) - C_o$ is defined via inverse liquidus slope ($\partial C / \partial T$) of quartz for particular system. Rhyolitic magma can be approximated by $\partial C_{qz} / \partial T \approx 0.001$ wt. fract. K^{-1} (defined using data from Johannes and Holtz, 1996) or $\Delta C \approx \Delta T \partial C_{qz} / \partial T \approx 0.1$ at $\Delta T = 100^\circ C$. The concentration parameter for zircon dissolution is defined not only by increasing temperature of the melt but also by dilution by rock-forming zirconium-free minerals through mass balance equation:

$$\Delta C = \frac{C(T_o + \Delta T)\epsilon_1 - C(T_o)\epsilon_o}{\epsilon_1}, \tag{14}$$

where $C(T)$ is solubility of $ZrSiO_4$ at the temperature T , $\epsilon -$ is a fraction of the melt in the magma. Solubility of zircon in the granite melt is well-constrained experimentally (Watson and Harrison, 1983). Typical value of ΔC associated with increasing of the melt fraction from $\epsilon = 0.35$ to $\epsilon = 0.75$ at heating from $750^\circ C$ to $850^\circ C$ is $2.5 \cdot 10^{-4}$. The characteristic radius R_0 links non-dimensional calculated distribution with a given natural CSD, it was set to $500\mu m$ for quartz and $50\mu m$ for zircon.

When we use diffusion coefficients of $3.9 \cdot 10^{-15} m^2/s$ for $850^\circ C$ and 4wt.% water, (recalculated from Acosta-Vigil et al., 2006 as described above) we obtain time necessary for dissolution of half of quartz crystals of 2 to 3.5yrs. Assuming similar water contents and temperatures, and taking diffusion and solubility model of zircon from Watson and Harrison, (1983) we obtain the corresponding dissolution–reprecipitation time to generate zircon’s CSD of 26yrs. In this calculation the melt fraction increases from 0.35 to 0.75 upon heating from 800 to $860^\circ C$. If we set heating from 760 to $800^\circ C$ with the same increase of the melt content time scales increases to 178years, because of the slower zirconium diffusion at lower temperatures.

4. Discussion

It is possible to check consistency of our interpretation of lognormal quartz CSDs measured in Bishop tuff (Bindeman, 2003; Gualda and Rivers, 2006) and modeled in this study with independent estimates of proportions of magmatic recycling derived from zoning of quartz crystals. Wark et al. (2007) measured cathodoluminescence (CL) intensity and TiO_2 concentrations in quartz phenocrysts and estimated temperature of their crystallization. They found that in the late sequence of Bishop quartz has high temperature overgrowth ($T = 800-820^\circ C$) over rounded dissolved cores ($T = 700-720^\circ C$). While heating and dissolution are explained by a basaltic intrusion, overgrowth at high temperature is explained by T–X– $X_{H_2O-CO_2}$ compositional relations specific to Bishop tuff. If their interpretation is correct, then this provides another degree of freedom in our model since the amount of the precipitated material is not directly defined by the amount of the dissolved at heating material but melting relations in the melt with variable water content. On published CL images of quartz crystals from the Late Bishop tuff (Peppard et al., 2001; Wark et al., 2007), only a few typically two to three dissolution surfaces can be seen. It is only evident that Late BT quartz underwent more severe dissolution and was precipitated due to water extraction into CO_2 bubbles and was not due to cooling. Residence time of the hot magma in the lower layer was estimated by Wark et al. (2007) through the shape of TiO_2 distribution on the boundary between core and overgrowth to be several hundreds years. It is semi-quantitatively consistent with our estimates based on the CSD analysis of the late BT CSD.

CL imaging of zircons in Yellowstone tuffs and lavas that collectively define lognormal CSD patterns also demonstrates rather simple zoning pattern (Bindeman et al., 2008). Isotopically diverse cores with variably dark CL and with diverse oxygen isotope values are surrounded by

light-CL, eruption-age rim, and investigation of zircon zoning patterns reveals that no more than two episodes of solution–reprecipitation has taken place. The remelting episodes are interpreted to represent blending different magma batches together followed by the pre-eruptive overgrowth by a single equilibrium rim. The amount of remelting based on CL imaging and also on oxygen isotope balance between cores and rims of bulk zircons is estimated to be in the 10–60% range. Based on oxygen isotope zoning, the time required to recycle zircons was estimated to be between $\sim 10^3$ and 10^4 years. It is possible that multiple solution–reprecipitation episodes recycled the outermost few percent of zircons but the last major episode of solution–reprecipitation erased the prior recycling memory, and truncated left side of the CSD to proportions required by the present model.

Let's consider experimental data on quartz and zircon with our theoretical estimates of the time evolution of CSDs. In experiments of Ayers et al. (2003) on zircon coarsening in water bearing quartzite, temperature was held constant at 1000°C. Initially crushed zircon crystal population annealed in “metamorphic conditions” via diffusion through the fluid phase distributed in the quartzite porous space. However, such annealing process is similar to the magmatic annealing because both are controlled by diffusion of nutrients through the melt/fluid and no gravity settling occurs. Experimental annealing of zircon by Ayers et al. (2003) yielded CSD shape that is close to log-normal distribution, similar to what is observed in most natural examples (e.g. Bindeman, 2003). The lognormal shape with deficiency of the smallest crystals obtained in the CSD of zircon in annealing experiments differs significantly from the shape predicted by the LSW model showing small crystal size tail (see Fig. 1b).

For quartz, there are experimental data on quartz coarsening in granite melt that can be taken from a recent work by Cabane et al. (2001). These authors find that the mean radius of quartz crystals at recrystallization can be approximated as a power of time $R \propto t^k$ with $k \approx 0.2$. Again, our model of temperature fluctuations compares nicely with these experimental results: our estimate of k is 0.19 (see Fig. 6a). Moreover, mean volumetric content of crystals N_v varies with time exponent $-k = 0.41$ – 0.51 , in good agreement with our estimate 0.56 (see Fig. 6b). At the same time LSW model predicts $k = 0.5$ – 0.33 in the crystal size dependence that is substantially larger than observed experimental values. Obviously our model provides better fit to the observations than the ripening theory based on the LSW approach. Furthermore, the results and predictions of the present model provide background for experimental testing in order to verify that the presented solution with at all its assumptions and simplifications catches the essence of natural processes and provides time exponents of CSD evolution correctly in a wide parameters range.

5. Conclusions

- 1) The simplified model based on the size dependent dissolution rate for crystals in the melt and constant slow overgrowth rate is proposed here to describe evolution of the CSD in the series of the dissolution–precipitation events.
- 2) The model can explain abundant lognormal CSD of quartz and zircon in natural systems by solution–reprecipitation after only a few cycles of melting–crystallization.
- 3) Quartz and zircon CSD in the same sample may experience different proportions of the dissolution depending on particular composition–melting relations for each mineral and zirconium concentration affecting solubilities.
- 4) Predicted by the model duration of the dissolution stage of about 100 years for zircon based on the measured CSD for upper Bishop tuff unit is comparable with one extracted from the quartz zonality (Wark et al., 2007).
- 5) Power exponent of the mean radius growth with time obtained in experiments on the quartz maturation is close to the obtained in our model for series of the low-intensity dissolution–precipitation events.

Acknowledgements

AGS was partially supported by the RFBR grant # 07-05-00629, University of Oregon, and NSF-EAR 0537872). We thank Keith Putirka, and an anonymous reviewer for providing careful reviews of the paper.

Appendix A. Dissolution rate at diffusion control

It is well known that at the control of dissolution by diffusion dissolution rate is inversely proportional to the particle size (radius in spherical approximation). This is valid for various geometries, for illustration we consider solution for the steady-state diffusion for sphere. Assume that small spherical source is placed inside spherical shell and constant concentration is set on the surface of the internal sphere. Diffusion equation at steady-state is reduced to the Laplacian of concentration or in spherically symmetrical case:

$$\frac{d}{dR} \left(\frac{dC}{dR} R^2 \right) / R^2 = 0 \quad (A1)$$

Solution for the shell boundary conditions $C(R_0) = C_0$, $C(R_1) = C_1$ ($R_1 > R_0$) is

$$C(R) = \frac{C_1 R_1 - C_0 R_0}{R_1 - R_0} - \frac{(C_1 - C_0) R_0 R_1}{(R_1 - R_0) R} \quad (A2)$$

In the case of infinite space ($R_1 = \infty$) $C(R) = C_1 + R_0(C_0 - C_1) / R$. Strictly saying moving boundary of the dissolving core substantially complicates solution of the diffusion problem. Here for brevity we will neglect effect of the moving boundary that is physically reasonable for slow dissolution processes considered. Diffusion flux from the surface of particle is fed by the dissolution so that

$$D \frac{dC}{dR} = u_{dis} \frac{\rho_s}{\rho_l} (C_s - C_0), \quad u_{dis} = D \frac{C_0 - C_1}{R_0(C_s - C_0)} \frac{\rho_l}{\rho_s} \quad (A3)$$

where ρ_s and ρ_l are densities of the solid and melt respectively, D is diffusion coefficient, C_0 is content of dissolved component at infinity, C_0 is solubility and C_s is slow-diffusing component content. Dependence of radius of dissolving particle from time can be found by integration of Eq. (A3) by taking $u_{dis} = dR_0 / dt$. It is easy to show that

$$R_0(t) = \sqrt{R_0(0)^2 - 2D \frac{(C_0 - C_1) \rho_l}{(C_s - C_0) \rho_s} t} \quad (A4)$$

For finite distance between crystals finite R_1 should be kept, resulting in the model similar to the communicating neighbors. Diffusive flux from the dissolved particles immersed in the finite shell of the melt approximately (R_0 is indeed lessen) equals

$$q = \exp \left(- \frac{6DR_0 t}{(R_0 + 2R_1)(R_1 - R_0)^2} \right) \frac{(C_1 - C_0) R_1}{(R_1 - R_0) R_0} \quad (A5)$$

It is obvious that at $t = 0$ and $R_1 = \infty$ formula (A5) transforms into Eq. (A3).

Appendix B. Influence of the settling flow on the dissolution rate

At diffusion control the maximum dissolution rate is associated with large curvature (small particles or sharp edges of large ones). If melt has low enough viscosity crystals settle with appreciable velocity, diffusion mass-transfer is accelerated for the larger sinking particles. Diffusion field around sinking particle is affected by the Stokes liquid flow resulting in the increasing of the concentration gradients at

the particle surface and enhancing of the dissolution rate. The total diffusive flux from the settling particle scaled on the half of the steady diffusive flux from fixed sphere of the same diameter is called Sherwood number (She). The total flux (J) is integral of the local flux (q) over the particle surface:

$$q = -D \left(\frac{\partial C}{\partial r} \right), J = \int_S q ds \quad (B1)$$

Reference diffusive flux is defined as

$$J_o = \frac{D(C_g - C_0)S}{2R}, \quad (B2)$$

where S is surface of the particle, C_g is dissolving component concentration on the surface, C_0 is content in the infinity, then non-dimensional Sherwood number is:

$$She = \frac{J/S\Delta C}{D/2R} \quad (B3)$$

At the negligible flow Sherwood number becomes $She = 2$. Influence of flow can be estimated via parametric dependence of She from Peclet number equals settling rate scaled on the diffusion velocity scale:

$$Pe = RV_{sed}/D$$

For low Reynolds numbers (low velocity of flow allows to neglect with inertia effects in the liquid flow) and low Peclet numbers ($0 < Pe < 1000$) Brauer and Schmidt-Traub (1973) theoretically found relationship:

$$She = 2 + \frac{0.333Pe^{0.840}}{1 + 0.331Pe^{0.507}}, \quad (A2)$$

where Stokes sedimentation velocity $V_{sed} = 2R^2\Delta\rho_{sl}/9\eta$ can be used. This relationship is in agree with low Pe limit: $She = 2 + aPe$ and high Pe limit $She = aPe^{1/3}$ derived in Bowman et al. (1961) and Friedlander (1957).

To estimate influence of the settling effect on the dissolution rate in the silicic melt we set viscosity $\eta = .10^5$ poise and calculate Sherwood number for zircon and quartz crystals with variable size (see Fig. 5). In the size range of interest effect of the flow is weak enough to neglect with it as the first approximation.

References

- Acosta-Vigil, A., London, D., Morgan VI, G.B., Dewers, T.A., 2006. Dissolution of quartz, albite, and orthoclase in H_2O -saturated haplogranitic melt at $800^\circ C$ and 200MPa: diffusive transport properties of granitic melts at crustal anatexis conditions. *J. Petrol.* 47 (2), 231–254.
- Annen, C., Sparks, R.S.J., 2002. Effects of repetitive emplacement of basaltic intrusions on thermal evolution and melt generation in the crust. *Earth Planet. Sci. Lett.* 203, 937–955.
- Anderson, A.T., Davis, A.M., Lu, F., 2000. Evolution of Bishop Tuff rhyolitic magma based on melt and magnetite inclusions and zoned phenocrysts. *J. Petrol.* 41, 440–473.
- Ayers, J.C., Delacruz, K., Miller, C., Switzer, O., 2003. Experimental study of zircon coarsening in quartzite – H_2O at 1.0GPa and $1000^\circ C$, with implications for geochronological studies of high-grade metamorphism. *Am. Mineral.* 88, 365–376.
- Baker, D.R., 1991. Interdiffusion of hydrous dacitic and rhyolitic melts and the efficacy of rhyolite contamination of dacitic enclaves. *Contrib. Mineral. Petrol.* 106, 462–473.
- Bindeman, I.N., 2003. Crystal sizes in evolving silicic magma chambers. *Geology* 31, 367–370.
- Bindeman, I.N., 2005. Fragmentation phenomena in populations of magmatic crystals. *Am. Mineral.* 90 (11–12), 1801–1815.
- Bindeman, I.N., Fu, B., Kita, N., Valley, J.W., 2008. Origin and evolution of Yellowstone silicic magmatism based on ion microprobe analysis of isotopically-zoned zircons. *J. Petrol.* 49, 163–193.
- Blundy, J., Cashman, K., Humphreys, M., 2006. Magma heating by decompression-driven crystallization beneath andesite volcanoes. *Nature* 443 (7107), 76–80.
- Bowman, C.W., Ward, D.M., Johnson, A.I., Trass, O., 1961. Mass transfer from fluid and solid spheres at low Reynolds numbers. *Can. J. Chem. Eng.* 2, 9–13.
- Brandeis, G., Marsh, B.D., 1989. The convective liquidus in a solidifying magma chamber: a fluid dynamic investigation. *Nature* 339, 613–616.
- Brauer, H., Schmidt-Traub, H., 1973. Kopplung von Stofftransport und chemischer Reaktion an Platten und Kugeln sowie in Poren. *Chem. Ing. Technik* 45, 341–344.
- Cabane, H., Laporte, D., Provost, A., 2001. Experimental investigation of the kinetics of Ostwald ripening of quartz in silicic melts. *Contrib. Mineral. Petrol.* 142, 361–373.
- Cabane, H., Laporte, D., Provost, A., 2005. An experimental study of Ostwald ripening of olivine and plagioclase in silicate melts: implications for the growth and size of crystals in magmas. *Contrib. Mineral. Petrol.* 150 (1), 37–53.
- Cashman, K.V., Ferry, J.M., 1988. Crystal size distribution (CSD) in rocks and the kinetics and dynamics of crystallization. 3. Metamorphic crystallization. *Contrib. Mineral. Petrol.* 99 (4), 401–415.
- Cashman, K.V., Marsh, B.D., 1988. Crystal size distribution (CSD) in rocks and the kinetics and dynamics of crystallization. 2. Makaopuhi lava lake. *Contrib. Mineral. Petrol.* 99 (3), 292–305.
- Cheng, H., Zhou, Z., Nakamura, E., 2008. Crystal-size distribution and composition of garnets in eclogites from the Dabie orogen, central China. *Am. Mineral.* 93, 124–133.
- Davidson, J.P., Morgan, D.J., Charlier, B.L.A., 2007. Isotopic microsampling of magmatic rocks. *Elements* 3 (4), 253–259.
- Djamarani, K.M., Clark, I.M., 1997. Characterization of particle-size based on fine and coarse fractions. *Powder Technol.* 93, 101–108.
- Donaldson, C.H., 1976. Experimental investigation of olivine morphology. *Contrib. Mineral. Petrol.* 57 (2), 187–213.
- Eberl, D.D., Kile, D.E., Drits, V.A., 2002. On geological interpretations of crystal size distributions: constant vs. proportionate growth. *Am. Mineral.* 87 (8–9), 1235–1241.
- Friedlander, S.K., 1957. Mass and heat transfer to single spheres and cylinders at low Reynolds numbers. *AIChE J.* 3, 43–48.
- Gualda, G.A.R., 2006. Crystal size distributions derived from 3D datasets: sample size versus uncertainties. *J. Petrol.* 47 (6), 1245–1254.
- Gualda, G.A.R., Rivers, M., 2006. Quantitative 3D petrography using x-ray tomography: application to Bishop Tuff pumice clasts. *J. Volcanol. Geotherm. Res.* 154, 48–62.
- Gualda, G.A.R., Cook, D.L., Chopra, R., Qin, L., Anderson Jr., A.T., Rivers, M., 2004. Fragmentation, nucleation and migration of crystals and bubbles in the Bishop Tuff Rhyolitic Magma. *Transactions of the Royal Society of Edinburgh: Earth Sciences. Special volume, 5th Hutton Symposium on the Origin of Granites and Related Rocks*, pp. 358–375.
- Hammer, J.E., 2004. Crystal nucleation in hydrous rhyolite: experimental data applied to classical theory. *Am. Mineral.* 89 (11–12), 1673–1679.
- Harrison, T.M., Watson, E.B., 1983. Kinetics of zircon dissolution and zirconium diffusion in granitic melts of variable water-content. *Contrib. Mineral. Petrol.* 84 (1), 66–72.
- Higgins, M.D., 1998. Origin of anorthosite by textural coarsening: quantitative measurements of a natural sequence of textural development. *J. Petrol.* 39, 1307–1323.
- Higgins, M.D., 2006. Quantitative textural measurements in igneous and metamorphic petrology. Cambridge University Press. 270 pp.
- Higgins, M.D., Roberge, J., 2003. Crystal size distribution of plagioclase and amphibole from Soufriere Hills Volcano Montserrat: evidence for dynamic crystallization – textural coarsening cycles. *J. Petrol.* 44 (8), 1401–1411.
- Hort, M., 1998. Abrupt change in magma liquidus temperature because of volatile loss or magma mixing: effects on nucleation, crystal growth and thermal history of the magma. *J. Petrol.* 39, 1063–1076.
- Hoskin, P.W.O., Schaltegger, U., 2003. The composition of zircon and igneous and metamorphic petrogenesis. In: Hanchar, J.M., Hoskin, P.W.O. (Eds.), *Zircon. Rev. Mineral. Geochem.*, vol. 53, pp. 27–62.
- James, P.F., 1985. Kinetics of crystal nucleation in silicate glasses. *J. Non-Cryst. Solids* 73, 517–540.
- Jackson, K., Uhlmann, D., Hunt, J., 1967. On the nature of crystal growth from the melt. *J. Cryst. Growth* 1, 1–36.
- Jerram, D.A., Davidson, J.P., 2007. Frontiers in textural and microgeochemical analysis. *Elements* 3 (4), 235–238.
- Johannes, W., Holtz, F., 1996. *Petrogenesis and Experimental Petrology of Granitic Rocks*. Springer Verlag, Berlin-Heidelberg.
- Kile, D.E., Eberl, D.D., 2003. On the origin of size-dependent and size-independent crystal growth: influence of advection and diffusion. *Am. Mineral.* 88 (10), 1514–1521.
- Kolmogorov, A.N., 1941. On the lognormal distribution law of the dimensions of particles under pulverization. *Dokl. Akad. Sci. USSR* 31, 99–101.
- Lasaga, A.C., 1998. *Reaction kinetics in geosciences*. Princeton University Press, Princeton, New Jersey. 811 p.
- Lifshitz, I.M., Slyozov, V.V., 1961. The kinetics of precipitation from supersaturated solid solution. *J. Phys. Chem. Solids* 19, 35–50.
- Lofgren, G.E., 1980. Experimental studies on the dynamic crystallization of silicate melts. *Physics of Magmatic Processes*. Princeton University Press, pp. 487–551.
- Marsh, B.D., 1988. Crystal size distribution (CSD) in rocks and the kinetics and dynamics of crystallization. 1. Theory. *Contrib. Mineral. Petrol.* 99 (3), 277–291.
- Marsh, B.D., 1989. Magma chambers. *Annu. Rev. Earth Planet. Sci.* 17, 439–474.
- Marsh, B.D., 1998. On the interpretation of crystal size distributions in magmatic systems. *J. Petrol.* 39, 553–599.
- Mock, A., Jerram, D.A., Breitzkreuz, C., 2003. Using quantitative textural analysis to understand the emplacement of shallow-level rhyolitic laccoliths – a case study from Halle volcanic complex, Germany. *J. Petrol.* 44, 833–849.
- Mourtada-Bonnefoi, C.C., Laporte, D., 2004. Kinetics of bubble nucleation in a rhyolitic melt: an experimental study of the effect of ascent rate. *Earth Planet. Sci. Lett.* 218 (3–4), 521–537.
- Nemchin, A.A., Giannini, L.M., Bodorkos, S., Oliver, N.H.S., 2001. Ostwald ripening as a possible mechanism for zircon overgrowth formation during anatexis: theoretical constraints, a numerical model, and its application to pelitic migmatites of the Tickalara Metamorphics, northwestern Australia. *Geochim. Cosmochim. Acta* 65 (16), 2771–2787.

- Peppard, B.T., Steele, I.M., Davis, A.M., Wallace, P.J., Anderson, A.T., 2001. Zoned quartz phenocrysts from the rhyolitic Bishop Tuff. *Am. Mineral.* 86, 1034–1052.
- Poldervaart, A., 1956. Zircon in rocks: 2. Igneous rocks. *Am. J. Sci.* 254, 521–554.
- Putirka, K., Tepley, F. (Editors). (in press) *Minerals, Inclusions and Volcanic Processes. Reviews in Mineralogy and Geochemistry.*
- Scott, A.S., 2003. The method of characteristics with applications to conservation laws. *J. Online Math. Appl. (JOMA)* 3 February 2003.
- Simakin, A.G., Chevychelov, V.Yu., 1995. Experimental study of Fsp crystallization from the granite melt with different water content. *Geochemistry* 2, 216–238.
- Simakin, A.G., Botcharnikov, R., 2001. Degassing of stratified magma by compositional convection. *J. Volcanol. Geotherm. Res.* 105, 207–224.
- Tammann, G., 1898. Über die Abhängigkeit der Zahl der Kerne. *Z. Phys. Chem.* 25, 441–479.
- Sunagawa, I., 1984. Growth of crystals in Nature. *Materials of the Earth's Interior.* Tokyo. TERRAPUB. 63–105pp.
- Wark, D., Watson, E.N., 2006. TitanQ: a titanium-in-quartz geothermometer. *Contrib. Mineral. Petrol.* 152 (6), 743–754.
- Wark, D.A., Spear, F.S., Cherniak, D.J., Watson, E.B., 2007. Pre-eruption recharge of the Bishop magma system. *Geology* 35 (3), 235–238.
- Watson, E.B., Harrison, T.M., 1983. Zircon saturation revisited: temperature and compositional effects in a variety of crustal magma types. *Earth Planet. Sci. Lett.* 64, 295–304.
- Watson, E.B., Harrison, T.M., 2005. Zircon thermometer reveals minimum melting conditions on earliest Earth. *Science* 308 (5723), 841–844.
- Zhang, Y.X., Walker, D., Leshner, C.E., 1989. Diffusive crystal dissolution. *Contrib. Mineral. Petrol.* 102, 492–513.